

# Thermodynamics of one-dimensional spin-orbit-coupled bosonic model in deep insulating region

Bin Xi<sup>1,2,\*</sup>, Shijie Hu<sup>3,\*</sup>, Qiang Luo<sup>2</sup>, Jize Zhao<sup>4,†</sup> and Xiaoqun Wang<sup>5,2‡</sup>

<sup>1</sup>*College of Physics Science and Technology, Yangzhou University, Yangzhou 225002, China*

<sup>2</sup>*Department of Physics and Beijing Laboratory of Opto-electronic Functional Materials & Micro-nano Devices, Renmin University of China, Beijing 100872, China*

<sup>3</sup>*Department of Physics and Research Center Optimas, Technical University Kaiserslautern, 67663 Kaiserslautern, Germany*

<sup>4</sup>*Institute of Applied Physics and Computational Mathematics, Beijing 100088, China* and

<sup>5</sup>*Department of Physics and Astronomy, Shanghai Jiao Tong University, Shanghai 200240, China*  
(Dated: December 9, 2024)

We study the thermodynamics of an XYZ Heisenberg chain with Dzyaloshinskii-Moriya interaction, which describes the low-energy behaviors of a one-dimensional spin-orbit-coupled bosonic model in the deep insulating region. The entropy and the specific heat are calculated numerically by the quasi-exact transfer-matrix renormalization group. In particular, in the limit  $U'/U \rightarrow \infty$ , our model is exactly solvable and thus serves as a benchmark for our numerical method. From our data, we find that for  $U'/U > 1$  a quantum phase transition between an (anti)ferromagnetic phase and a Tomonaga-Luttinger liquid phase occurs at a finite  $\theta$ , while for  $U'/U < 1$  a transition between a ferromagnetic phase and a paramagnetic phase happens at  $\theta = 0$ . A refined ground-state phase diagram is then deduced from their low-temperature behaviors. Our findings provide an alternative way to detect those distinguishable phases experimentally.

PACS numbers:

## I. INTRODUCTION

One-dimensional (1D) quantum magnetism remains an active research area in condensed matter physics because of their intriguing properties arising from strong quantum fluctuations<sup>1</sup>. Among them, the 1D spin-1/2 antiferromagnetic (AF) Heisenberg chain is a prototypical model, the ground state of which is a Tomonaga-Luttinger liquid (TLL)<sup>2</sup>. It has gapless elementary excitations and is relevant to a variety of quasi-1D magnetic materials<sup>3–5</sup>. However, its properties may change significantly in the presence of anisotropy<sup>6–8</sup>.

In addition to abundant quasi-1D materials, ultracold atomic systems in optical lattices have already become an important platform to simulate quantum spin systems. Spin-spin interaction using controlled collisions was first proposed<sup>9</sup> theoretically in 1999 and later successfully realized in experiments with <sup>87</sup>Rb atoms of two hyperfine states<sup>10</sup>. In these experiments, the two states  $|F = 1, m_F = -1\rangle$  and  $|F = 2, m_F = -2\rangle$  are treated as up and down spins<sup>10</sup>, respectively. This two-component boson mixture soon attracted great interests. Duan and coworkers suggested that the Hamiltonian of this two-component system can be mapped into a spin-1/2 XXZ Heisenberg model<sup>11</sup>. Its ground state is ferromagnetic (FM) when intercomponent interaction  $U'$  is much larger than intracomponent one  $U$ , while it is AF when  $U' \ll U$ . These studies have provided us valuable information to understand some long-standing problems in condensed matter physics. Recently, more complicate spin models have been proposed in the basis of optical lattice. For example, it was demonstrated that XYZ Heisenberg models can be implemented with p orbit bosons<sup>12</sup> in one dimen-

sion, and with Rydberg atoms in two dimensions<sup>13,14</sup>.

An artificial spin-orbit coupling (SOC), or equivalently, gauge field, was successfully realized in experiments and a variety of phases as well as phase transitions have been observed<sup>15–18</sup>. These experiments have spurred a great deal of interest in studying the artificial SOC as well as gauge field in ultracold systems<sup>19–34</sup>. In particular, in the deep insulating region, such an SOC can be approximated<sup>21,26</sup> by Dzyaloshinskii-Moriya (DM) interaction<sup>35,36</sup>. In many magnetic materials, DM interaction plays a key role in understanding a variety of exotic magnetic features, e.g. spiral magnetism<sup>19–21,37</sup>, skyrmion<sup>38–42</sup>. Therefore, it is expectable that rich and complicated magnetic structure can be experimentally observed in ultracold atomic systems with the SOC.

The SOC realized in 2011 has equal weight of Rashba and Dresselhaus terms. Thus it is along one direction in real space. Loaded into one-dimensional optical lattice<sup>30</sup>, the low-energy dynamics of spin-orbit coupled bosons can be modeled by the Hamiltonian<sup>25</sup>

$$\hat{\mathcal{H}}_{\text{boson}} = \hat{\mathcal{K}} + \hat{\mathcal{T}}_{\text{soc}} + \frac{U}{2} \sum_{i\tau} \hat{n}_{i\tau}(\hat{n}_{i\tau} - 1) + U' \sum_i \hat{n}_{i\uparrow} \hat{n}_{i\downarrow}, \quad (1)$$

where  $\hat{\mathcal{K}} = -t \sum_{i\tau} (\hat{c}_{i\tau}^\dagger \hat{c}_{i+1\tau} + \text{H.c.})$  is the hopping term between nearest-neighbor sites,  $\hat{\mathcal{T}}_{\text{soc}} = -\lambda \sum_i (\hat{c}_{i\uparrow}^\dagger \hat{c}_{i+1\downarrow} - \hat{c}_{i\downarrow}^\dagger \hat{c}_{i+1\uparrow} + \text{H.c.})$  describes the SOC.  $\hat{c}_{i\tau}^\dagger$  ( $\hat{c}_{i\tau}$ ) is the creation (annihilation) operator at site  $i$  with spin  $\tau$ .  $\tau$  takes  $\uparrow$  and  $\downarrow$ , representing two internal states of atoms.  $U$  is on-site intracomponent interaction and  $U'$  is the intercomponent one.  $\hat{n}_{i\tau} = \hat{c}_{i\tau}^\dagger \hat{c}_{i\tau}$  is the boson number operator with spin

$\tau$  at site  $i$ .  $\mu$  is the chemical potential to control the filling factor. At unit filling and in strong coupling limit  $t, \lambda \ll U$ , this model can be effectively written as an XYZ Heisenberg chain with the DM interaction (see Ref.<sup>26</sup> for more details). By setting  $t = J \cos \theta$ ,  $\lambda = J \sin \theta$ , it reads:

$$\hat{\mathcal{H}} = \frac{4J^2}{U} \left[ \left( -2 + \frac{U}{U'} \right) \cos 2\theta \sum_i \hat{S}_i^z \hat{S}_{i+1}^z - \frac{U}{U'} \cos 2\theta \sum_i \hat{S}_i^x \hat{S}_{i+1}^x - \frac{U}{U'} \sum_i \hat{S}_i^y \hat{S}_{i+1}^y - \sin 2\theta \sum_i (\hat{S}_i^z \hat{S}_{i+1}^x - \hat{S}_i^x \hat{S}_{i+1}^z) \right], \quad (2)$$

where  $\hat{S}_i^\nu = \sum_{\tau\tau'} \hat{c}_{i\tau}^\dagger \hat{\sigma}_{\tau\tau'}^\nu \hat{c}_{i\tau'}$  are the pseudo-spin operators with  $\hat{\sigma}^\nu$  Pauli matrix and  $\nu = x, y, z$ .

The Hamiltonian (2) has been studied by several groups using density-matrix renormalization group (DMRG) method in combination with some analytic methods<sup>25–29</sup>. For  $U' = U$ , the DM interaction can be eliminated by a site-dependent rotation of the spin operators, resulting in an isotropic Heisenberg chain with FM coupling<sup>20</sup>. In this sense, the SOC becomes trivial in such case. However, when  $U' \neq U$ , the DM interaction cannot be simply eliminated and several phases have been predicted. For  $U' > U$ , there are a gapped FM phase, a gapped AF phase, and a TLL phase with a chiral order in between<sup>26</sup> (without ambiguity, we will call it TLL phase below). The transition from the FM (AF) phase to the TLL phase is of first order. For  $U' < U$ , a gapless paramagnetic phase and a gapful FM phase are found<sup>25</sup>. The transition between these two phases is of Berezinskii-Kosterlitz-Thouless(BKT) type<sup>43</sup>. However, due to the limit of numerical accuracy and finite-size effect, the critical point has not been determined accurately.

By far, the study of Hamiltonian (2) is still limited to zero temperature. Its properties at finite temperature remain unknown yet. In particular, when approaching zero temperature, what are the asymptotic behaviors of some typical quantities such as entropy, specific heat? Understanding these issues is remarkably important for determining phase diagram experimentally. On the other hand, Hamiltonian (2) is quite general although it originates from the context of ultracold systems. We believe that it is qualitatively relevant to some quasi-1D materials, such as Copper benzoate<sup>44</sup>,  $\text{Cs}_2\text{CoCl}_3$ <sup>45</sup>,  $\text{CuCl}_2 \cdot 2(\text{dimethylsulfoxide})$  (CDC)<sup>46,47</sup>, copper pyrimidine<sup>48–50</sup> and  $\text{Yb}_4\text{As}_3$ <sup>51</sup>.

In this work, we study the thermodynamics of the Hamiltonian (2) with transfer-matrix renormalization group (TMRG) method<sup>52</sup>. TMRG is a powerful numerical method for studying the thermodynamics of one-dimensional quantum systems. We refer the reader to references<sup>52–55</sup> for more details. During the TMRG iterations, 1000  $\sim$  2000 states are kept in most cases. The truncation error is less than  $10^{-12}$  in all calculations. Particularly, we use an additional reorthogonalization

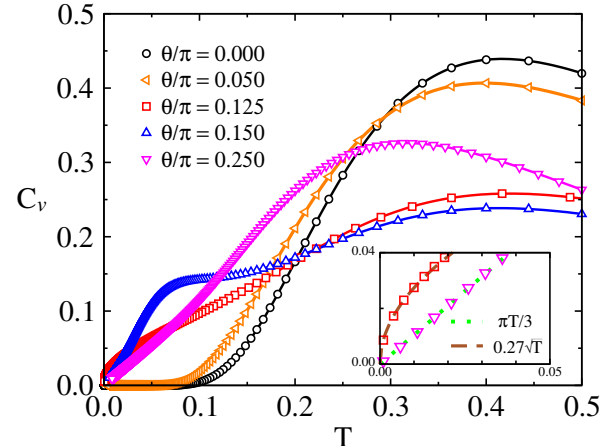


FIG. 1: (color online). Exact solutions (lines) and TMRG results (symbols) of the specific heat are plotted as a function of temperature  $T$  for a variety of  $\theta$ . Inset shows asymptotic behavior of the specific heat at low temperature for two different cases: 1)  $\theta = \pi/4$  ( $\nabla$ ) corresponding to the TLL phase, the specific heat is proportional to  $T$  and 2)  $\theta = \pi/8$  ( $\square$ ) at which the transition takes place between the TLL and a gapped FM phase, it behaves as  $\sqrt{T}$ .

sation procedure after the left and right eigenvectors of the reduced density matrix are obtained. This allows us to keep more states and thus improve accuracy<sup>56</sup>. For simplicity, we set  $4J^2/U$  as the energy unit. One can immediately see that Hamiltonian (2) has period  $\pi/2$  in  $\theta$  by performing such a transformation  $\hat{S}_{2i+1}^x \rightarrow -\hat{S}_{2i+1}^x$ ,  $\hat{S}_{2i+1}^y \rightarrow \hat{S}_{2i+1}^y$  and  $\hat{S}_{2i+1}^z \rightarrow -\hat{S}_{2i+1}^z$ . Moreover, one can interchange  $t$  and  $\lambda$  in Hamiltonian (1)<sup>25,31</sup>, so we only need to consider the parameter region  $\theta \in [0, \pi/4]$  since the properties in the region  $(\pi/4, \pi/2]$  are readily available.

The paper is organized as follows: in Section II, we begin our study in the exactly solvable limit  $U'/U \rightarrow \infty$ . In Section III, we consider the region  $U'/U > 1$ . The phase transition points are obtained through the isentropy map. In the low-temperature limit, the asymptotic behaviors in different phases are compared. In Section IV, we focus on the system in the region  $U' < U$ . We determine the critical point from the entropy. In Section IV, we give our conclusions.

## II. EXACTLY SOLVABLE CASE

In the limit  $U'/U \rightarrow \infty$ , Hamiltonian (2) is reduced to

$$\hat{\mathcal{H}} = -2 \cos 2\theta \sum_i \hat{S}_i^z \hat{S}_{i+1}^z - \sin 2\theta \sum_i (\hat{S}_i^z \hat{S}_{i+1}^x - \hat{S}_i^x \hat{S}_{i+1}^z). \quad (3)$$

One can see immediately that at  $\theta = 0$  the Hamiltonian (3) is just an Ising model with a FM ground state, while

at  $\theta = \pi/4$  it is equivalent to an isotropic XY model with a TLL ground state. For general  $\theta$ , the Hamiltonian (3) can be transformed into a Kitaev chain by the Jordan-Wigner transformation<sup>57</sup>, which is exactly solvable, leading to  $\hat{\mathcal{H}} = \sum_k E_k (\hat{\Lambda}_k^\dagger \hat{\Lambda}_k - 1/2)$  with the energy dispersion  $E_k = \cos 2\theta - \sin 2\theta \sin k$  and  $\hat{\Lambda}_k^\dagger$  ( $\hat{\Lambda}_k$ ) the creation (annihilation) operator of fermions (see Appendix A for more details). One can notice that the system undergoes a quantum phase transition from a gapped phase into a gapless one at  $\theta = \pi/8$ . The thermodynamic properties of the Hamiltonian (3) can then be exactly calculated from the dispersion  $E_k$  through the partition function  $Z$  in a standard way. For example, the specific heat can be expressed by the definition in the continuum limit as

$$\begin{aligned} C_v &= \beta^2 \frac{\partial^2 \ln Z}{\partial \beta^2} \\ &= \frac{1}{2\pi} \int_{-\pi}^{\pi} dk (\beta E_k/2)^2 \cosh^{-2}(\beta E_k/2), \end{aligned} \quad (4)$$

with  $\beta$  the inverse temperature.  $C_v$  can be evaluated exactly after completing numerical integration. The results are shown in Fig. 1 together with our TMRG results. One can see that our TMRG results agree well with the exact ones, verifying the precision of the TMRG data.

The low-temperature behavior of specific heat reveals distinguishable features for different values of  $\theta$ . At  $\theta = 0$ , The system is just a classical Ising chain and  $E_k \equiv 1$ . One can easily obtain  $C_v = (\beta/2)^2 \cosh^{-2}(\beta/2)$ , which can be approximate to  $T^{-2} \exp(-1/T)$  under low- $T$  limit. For  $0 < \theta < \pi/8$ , though the ground state is also an Ising-type FM phase, the low-temperature behavior is different. Here the low-energy excitations are governed by the gapful magnon dispersion, which can be approximately written as

$$\epsilon_q = \Delta + \frac{1}{2} \sin 2\theta q^2 + O(|q|^3), \quad (5)$$

where  $q = k - \pi/2$  and  $\Delta = \cos 2\theta - \sin 2\theta$  is the energy gap between the ground state and the first excitation at  $k = \pi/2$ . The  $q^2$ -dependence of the magnon dispersion results in  $C_v \sim T^{-3/2} \exp(-\Delta/T)$  for  $T \ll \Delta$ <sup>55</sup>. These two different exponential behaviors are shown in Fig. 1 with  $\theta = 0$  and  $0.05\pi$ . At  $\theta = \pi/8$ , a phase transition takes place between the gapful FM phase and the TLL. Though the gap is closed at this point, the low energy excitation is still proportional to  $q^2$ , and one has the density of states as  $g(E_{\pi/2}) \sim dk/dE|_{k=\pi/2} \sim 1/\sqrt{E_{\pi/2}}$ . It turns out that the free energy  $F$  reads

$$\int dE \frac{Eg(E)}{\exp(E/k_B T) + 1} \sim T^{3/2}, \quad (6)$$

which leads to a  $T^{1/2}$ -dependence of the specific heat as shown in the inset of Fig.1. In the TLL phase corresponding to  $\theta > \pi/8$ , one has effectively a Fermi momentum  $k_F = \arcsin(\tan 2\theta)$ , which moves from  $\pi/2$  towards 0 with further increasing  $\theta$  from the transition point. As

a consequence, the specific heat involves a bump at low temperature and becomes linear in the very low  $T$  regime. An example is given for  $\theta/\pi = 0.15$  shown in Fig.1. The bump reflects the contribution from the dispersion deviating from the linearity of the TLL. This causes characteristically a crossover in specific heats between an ideal TLL phase which has purely linear excitations and other phases with  $k^2$ -excitations. The bump shifts to higher temperature with respect to increasing of  $\theta$  and is eventually absorbed by the peak of the specific heat when  $\theta = \pi/4$ . In the TLL phase, low energy excitations are proportional to the momentum  $\delta k$ , which results in a  $T^2$ -dependence of free energy at very low temperature so that one has  $C_v/T = \pi/3v$  where  $v$  is the spin-wave velocity<sup>58</sup> and equals to  $\sqrt{-\cos 4\theta}$  for the present case. Therefore one can obtain the following low temperature behavior for the specific heat:

$$C_v = \frac{\pi}{3\sqrt{-\cos 4\theta}} T. \quad (7)$$

The inset of Fig. 1 illustrates this behavior for  $\theta = \pi/4$  as compared with TMRG results.

### III. $U'/U > 1$

After benchmarking our TMRG method, we now turn to our main task, anisotropic interacting case, i.e.,  $U'/U$  is finite but  $U'/U \neq 1$ . Under this condition, the Hamiltonian is not simply solvable, and thus we resort to the TMRG method to study it. In this section, we focus on  $U'/U > 1$ .

#### A. Entropy

The location of the transition point can be determined through the isentropic map. It is known that, at the same temperature,  $S$  has a maximum at the transition point. As a result, all the isentropic curves should bend to the transition point. As shown in Fig. 2, one can easily figure out that at  $U'/U = 1.2$  the transition point locates at  $\theta/\pi = 0.072(1)$ , which agrees well with previous results obtained by DMRG method<sup>26</sup>. Meanwhile, we notice that the isentropic map shows a clear cooling process similar to magnetocaloric effect (MCE) in magnetic materials<sup>59</sup>. Starting from  $T_i$  and decreasing  $\theta$ , one can design an isothermal process of entropy decreasing (black arrow). Then following an isentropic curve with increasing  $\theta$  (red arrow), it is allowed to decrease the temperature gradually to  $T_f$ . Here the strength of SOC is used instead of magnetic field in usual MCE. The entropy is transferred from gapless states to gapped states in the isothermal process, then followed by a gap closing in the isentropic process. As a contrast, common MCE in magnetic materials contains an isothermal suppression of the entropy from disordered phases to FM ordered phases,

then followed by an adiabatic demagnetization<sup>59</sup>. In ultracold systems, a common way for lowering the temperature of the quantum gas is transferring the entropy from the ground band to higher bands and removed<sup>60</sup>. The possibility and efficiency of using the MCE-like process as an alternative technology for refrigeration in cold atom systems needs further experimental investigations.

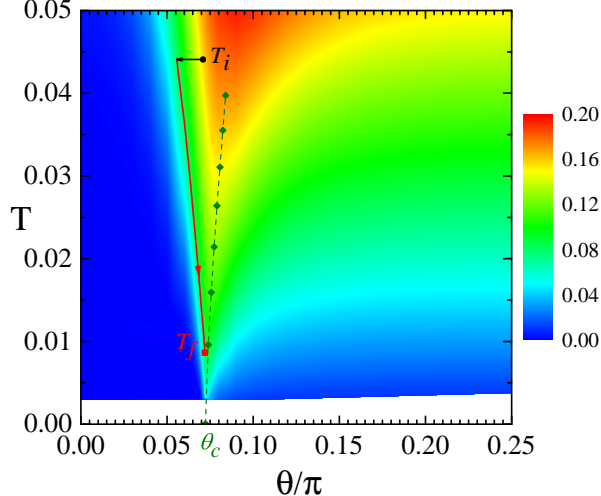


FIG. 2: (color online). Isentropic map of  $S(\theta, T)$  at  $U'/U = 1.2$ . The color represents the value of  $S$ . The transition point can be directly obtained through tips of isentropic curves. A cooling process from  $T_i$  to  $T_f$  similar to MCE is shown. The black arrow is an isothermal line of entropy decreasing, and the red arrow is an isentropic line with gap closing, revealing a MCE-like process.

## B. Specific heat

In Fig. 3, we plot the specific heat as a function of temperature for a variety of  $\theta$  at  $U'/U = 1.2$ , which is qualitatively similar to the results in the exactly solvable limit. However, at  $\theta = 0$ , the system is now a gapped XXZ model, and the specific heat at low temperature is  $C_v \sim T^{-3/2} \exp(-\Delta/T)$ . At the transition point  $\theta = \theta_c \simeq 0.072$ , our numerical data show that it deviates from the square-root behavior, which suggests that the dispersion of the low-energy excitations is not well approximated by  $k^2$  for a finite  $U'/U$ . For  $\theta > \theta_c$ ,  $C_v \sim T$ , which is a characteristic feature of TLL.

The transition points can be determined from the finite-temperature scaling of the specific heat as well<sup>61,62</sup>. In Fig. 4, we present a contour plot of the specific heat with  $T$  and  $\theta$ . For each fixed  $T$ , one can obtain three extreme points  $C_v^e$  with two maximums and one minimum. The corresponding locations of  $T_e$  and  $\theta_e$  should follow a scaling behavior<sup>61,62</sup>:

$$T_e \propto |\theta_e(T) - \theta_c|^\alpha,$$

with  $\theta_c$  the transition point and  $\alpha$  the critical exponent. The fitting dashed lines in Fig. 4 show rather good linear

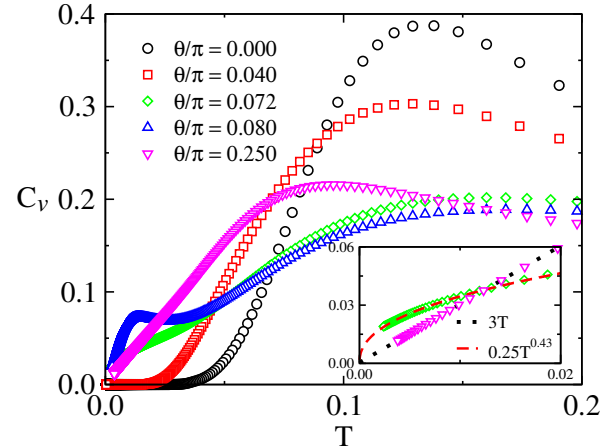


FIG. 3: (color online). Specific heat as a function of temperature obtained by TMRG for a variety of  $\theta$  at  $U'/U = 1.2$ .

behaviors, indicating  $\alpha = 1$ . Furthermore, the transition point is fitting to  $\theta_c = 0.072(1)$ , which agrees well with that we obtain from the entropy.

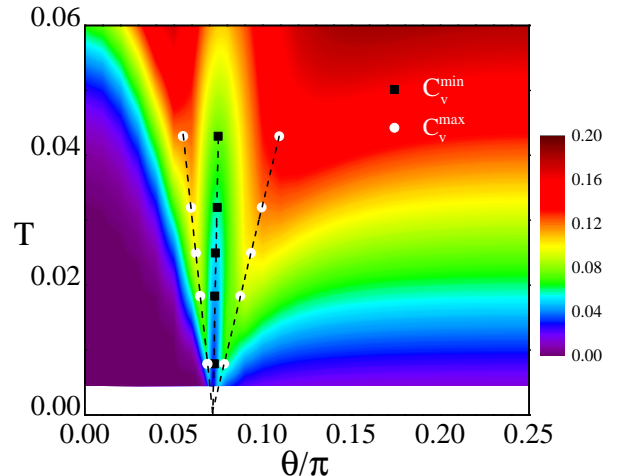


FIG. 4: (color online). Contour plot of specific heat  $C_v(T, \theta)$ . Symbols are the extreme points and dashed lines are fitting curves.

Fisher and Berker have established the scaling description of classical first-order phase transitions<sup>63</sup>. Subsequent works show its validity in the quantum ones<sup>64,65</sup>. We notice the scaling relation  $\alpha = 1$  has also been found at the transition point  $\Delta = -1$  in a 1d spin-1/2 XXZ chain, where the first-order phase transition separates the FM and TLL phases<sup>66</sup>. Since the symmetry of these two model is quite different, this resemblance deserves further theoretical analysis.

## IV. $U'/U < 1$

As shown in the the ground-state phase diagram given by Zhao et al.<sup>25</sup>, in this case, there are two phases, a

paramagnetic phase and a FM one. The former is gapless while the latter is gapful. The transition between these two phases are of BKT type<sup>43</sup>. In the BKT transition, it is a big challenge to figure out the critical point accurately. To determine the phase boundary, the entanglement entropy of the ground state of the Hamiltonian (1) was calculated<sup>25</sup> by DMRG. An extrapolation from the maximum of entanglement entropy for various system sizes was made. Based on their analysis, the transition seems to occur at a finite  $\theta$  for a finite  $U'$ . Another DMRG calculation based on the effective model (2) gives a relatively large error bar for the position of the critical points<sup>27</sup>. In this section, we will study the thermodynamical properties, from which we can provide strong numerical evidence that the transitions from the paramagnetic phase to the FM phase occur at  $\theta = 0$ .

### A. Entropy

In this subsection, we will discuss the entropy. For simplicity, we limit our discussion to  $U'/U = 0.5$ . In Fig. 5, we plot the isentropic map. In contrast to the case  $U'/U > 1$ , we do not find any singular point on the isentropic curves at finite  $\theta$ . Moreover, we observe

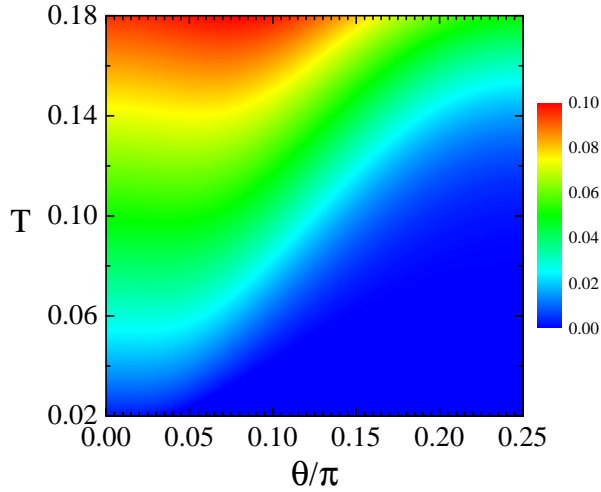


FIG. 5: (color online). Isentropic map of  $S(T, \theta)$  at  $U'/U = 0.5$ . The color represents the value of entropy at given  $\theta, T$ .

that the entropy near the left is larger than that on the right at low temperature. This can be understood from the known results that the FM phase is gapful while the paramagnetic phase is gapless. As temperature increases, the isentropic curve becomes flatter. This is because at high temperature the thermal fluctuation dominates over the quantum fluctuation. To extract the critical point between such gapped and gapless phases, we first determine the position  $\theta_m$  where the entropy is maximum for a fixed temperature, and then extrapolate them to zero temperature. In Fig. 6, we plot  $\theta_m$  as a function of the temperature  $T$ . The curve can be well fitted by a linear

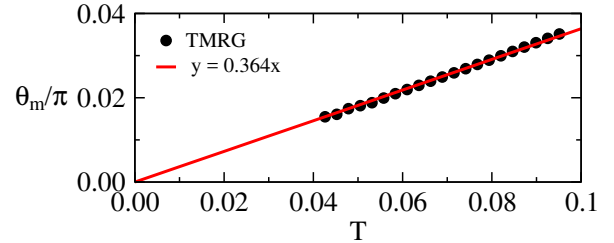


FIG. 6: (color online). Extrapolation of  $\theta_m$  which has the maximal entropy at given temperatures to determine the critical value.

function  $\theta_m = a \cdot T$ , with the parameter  $a = 0.364(2)$ . Thus, we conclude that within our error bar the critical point locates at  $\theta_c = 0$ . In Appendix B, we perform a DMRG calculation, which leads to the same conclusion.

### B. Specific Heat

In Fig. 7(a), we plot the specific heat as a function of temperature for a variety of  $\theta$  at  $U'/U = 0.5$ , which is much different from the results of  $U'/U > 1$ . At low temperature,  $C_v$  decreases exponentially (linearly) in the gapped (gapless) phases. One can see that the energy gap increases as  $\theta$  grows. Furthermore, it is interesting to find that all the specific heat curves  $C_v(T, \theta)$  intersect approximately at one point  $T^* \approx 0.527(3)$ . Such a crossing point is called isosbestic point, which has been theoretically analyzed with  $C_v(T, U)$  curves of Hubbard models<sup>67</sup>. This unique feature has been widely observed in many experiments, such as: specific heat of normal-fluid  $^3\text{He}$ <sup>68</sup> and heavy-fermion systems<sup>69,70</sup>, dielectric constant and optical conductivity in High-T<sub>c</sub> superconductor  $\text{Rb}_{11x}\text{Fe}_{2y}\text{Se}_2$ <sup>71</sup> and photoemission spectra of thin  $\text{VO}_2$  films<sup>72</sup>. Following the argument given by Vollhardt<sup>73</sup>, we can expand  $C_v(T, \theta)$  as:

$$C_v(T, \theta) = C_v(T, 0) + \cos^2(2\theta)F(T) + O[\cos^3(2\theta)],$$

where

$$F(T) \approx \frac{C_v(T, \theta_1) - C_v(T, \theta_2)}{\cos^2(2\theta_1) - \cos^2(2\theta_2)},$$

is a function of  $T$  only. The validity of this expansion can be verified by

$$\tilde{C}_v(T) = C_v(T, \theta) - \cos^2(2\theta)F(T) \approx C_v(T, 0).$$

As shown in Fig. 7(b), all specific heat curves for different  $\theta$  collapse well into a single curve at high temperature. We have confirmed that such isosbestic point can be observed for  $U'/U \gtrsim 0.45$  in our model.

## V. CONCLUSIONS

In conclusion, we study the thermodynamics properties of a spin-1/2 XYZ Heisenberg chain with a DM inter-

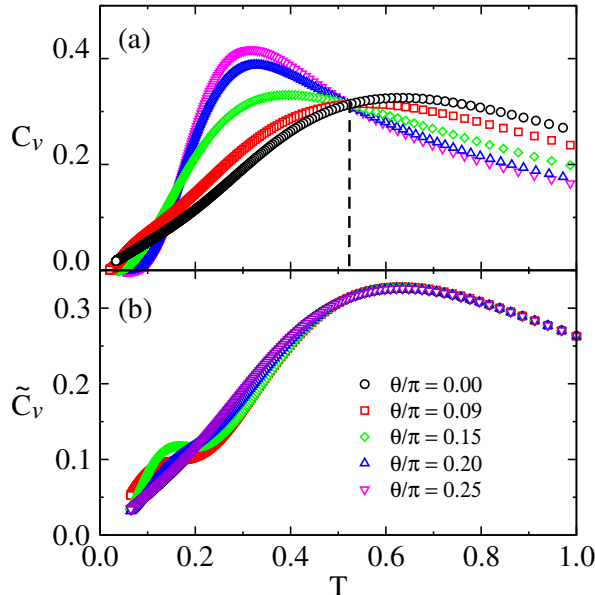


FIG. 7: (color online). (a) Specific heat as a function of temperature for a variety of  $\theta$  at  $U'/U = 0.5$ . An isosbestic point is indicated by dashed line. (b) Scaled specific heat  $\tilde{C}_v(T)$  collapses into one line at high temperature.

action by using the TMRG method. This model approximates the two-component Bose-Hubbard model with a synthetic SOC in deep insulating region. For  $U'/U > 1$ , the specific heat and entropy show three different asymptotic behaviors, depending on the phases at zero temperature. Moreover, we determine the transition points between the gapless TLL phase and the FM(AF) phase through the isentropic map. The MCE-like process as well as the scaling behavior near transition point is discussed. On the other hand, for  $U'/U < 1$ , we find no singularity in the isentropic map at finite  $\theta$ . After analysing our data carefully, we determine that the transition between the paramagnetic phase and the FM phase occurs at  $\theta = 0$ . We confirm this conclusion by DMRG calculations. Based on our results, a refined ground-state phase diagram is given in Fig. 8.

## VI. ACKNOWLEDGEMENTS

We thank Wei Li for helpful discussion. This work was supported by the National Natural Science Foundation of China (Grants No. 11474029, 11574200), by MOST 2016YFA0300500, by the Special Program for Applied Research on Super Computation of the NSFC-GD Joint Fund, and by the SFB Transregio 49 of the Deutsche Forschungsgemeinschaft (DFG) and the Allianz für Hochleistungsrechnen Rheinland-Pfalz (AHRP).

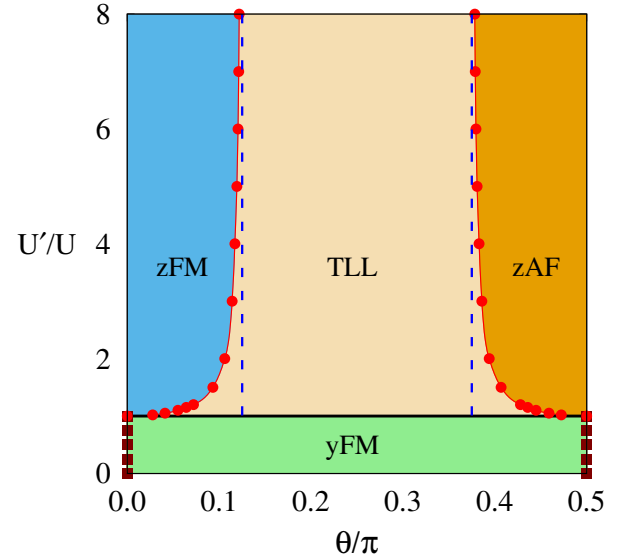


FIG. 8: (color online). Ground state phase diagram of Hamiltonian (2) in the  $U'/U$  vs  $\theta$  plane. The two exact transition points in the  $U'/U \rightarrow \infty$  limit are indicated by blue dashed lines, locating at  $\theta = \pi/8$  and  $\theta = 3\pi/8$ . For  $U'/U > 1$ , the red circles are the transition points between zFM (zAF) phase and TLL phase, and the solid red lines are guide to eyes. At  $U'/U = 1$ , it is a spiral phase. For  $U'/U < 1$ , the transition between the paramagnetic phase and the yFM phase occurs at  $\theta = 0$  and  $\theta = 0.5\pi$ , as marked by maroon squares. The lowercase letters y,z are the polarization directions.

## Appendix A: Exact solution in the $U'/U = \infty$ limit

The effective Hamiltonian (2) in the limit  $U'/U \rightarrow \infty$  can be reduced to

$$\hat{\mathcal{H}} = -J \sum_i \hat{S}_i^z \hat{S}_{i+1}^z - D \sum_i (\hat{S}_i^z \hat{S}_{i+1}^x - \hat{S}_i^x \hat{S}_{i+1}^z), \quad (\text{A1})$$

with  $J = 2 \cos \theta \geq 0$  and  $D = \sin 2\theta \geq 0$ . The exact solution<sup>57</sup> of (A1) is obtained by the Jordan-Wigner (JW) transformation.

The Hamiltonian is invariant under the rotation

$$\left\{ \begin{array}{l} \hat{S}^x \rightarrow \hat{S}^y \\ \hat{S}^y \rightarrow \hat{S}^z \\ \hat{S}^z \rightarrow \hat{S}^x \end{array} \right\} \quad (\text{A2})$$

and accordingly, (A1) turns into

$$\hat{\mathcal{H}} = -J \sum_i \hat{S}_i^x \hat{S}_{i+1}^x - D \sum_i (\hat{S}_i^x \hat{S}_{i+1}^y - \hat{S}_i^y \hat{S}_{i+1}^x). \quad (\text{A3})$$

By the definition

$$\left\{ \begin{array}{l} \hat{c}_j^\dagger = e^{-i\pi \sum_{n < j} \hat{S}_n^+ \hat{S}_n^-} \hat{S}_j^+ \\ \hat{c}_j = e^{i\pi \sum_{n < j} \hat{S}_n^+ \hat{S}_n^-} \hat{S}_j^- \end{array} \right. \quad (\text{A4})$$

with  $\hat{S}^+ = (\hat{S}^x + i\hat{S}^y)/2$  and  $\hat{S}^- = (\hat{S}^x - i\hat{S}^y)/2$ , we have

$$\begin{cases} \hat{S}_i^x \hat{S}_{i+1}^x = \frac{1}{4} (\hat{c}_i^\dagger \hat{c}_{i+1}^\dagger + \hat{c}_i^\dagger \hat{c}_{i+1} - \hat{c}_i \hat{c}_{i+1}^\dagger - \hat{c}_i \hat{c}_{i+1}) \\ \hat{S}_i^x \hat{S}_{i+1}^y - \hat{S}_i^y \hat{S}_{i+1}^x = \frac{1}{2i} (\hat{c}_i^\dagger \hat{c}_{i+1} + \hat{c}_i \hat{c}_{i+1}^\dagger) \end{cases} \quad (\text{A5})$$

The Hamiltonian (A3) finally becomes

$$\hat{\mathcal{H}} = - \sum_j \left( J^0 \hat{c}_i^\dagger \hat{c}_{i+1}^\dagger - J^0 \hat{c}_i \hat{c}_{i+1} + J^+ \hat{c}_i^\dagger \hat{c}_{i+1} - J^- \hat{c}_i \hat{c}_{i+1}^\dagger \right), \quad (\text{A6})$$

with  $J^0 = J/4$ ,  $J^\pm = (\frac{J}{2} \pm iD)/2$ . Here periodic boundary conditions are imposed. After Fourier transformation

$$\begin{cases} \hat{c}_k = \frac{1}{\sqrt{N}} \sum_j e^{ikj} \hat{c}_j \\ \hat{c}_k^\dagger = \frac{1}{\sqrt{N}} \sum_j e^{-ikj} \hat{c}_j^\dagger, \end{cases} \quad (\text{A7})$$

we obtain the Hamiltonian in the momentum space

$$\hat{\mathcal{H}} = \sum_k \left[ A(k) \hat{c}_k^\dagger \hat{c}_k + B(k) \left( \hat{c}_k^\dagger \hat{c}_{-k}^\dagger + \hat{c}_{-k} \hat{c}_k \right) \right], \quad (\text{A8})$$

with  $A(k) = -(J \cos k + D \sin k)/2$ ,  $B(k) = i \sin k/4$  and the following relations:

$$\begin{cases} \sum_k e^{-ik} \hat{c}_k^\dagger \hat{c}_{-k}^\dagger = -i \sum_k \sin k \hat{c}_k^\dagger \hat{c}_{-k}^\dagger \\ \sum_k e^{ik} \hat{c}_k \hat{c}_{-k} = i \sum_k \sin k \hat{c}_k \hat{c}_{-k} \end{cases} \quad (\text{A9})$$

The diagonalization is finished up by the Bogoliubov transformation:

$$\begin{cases} \hat{\Lambda}_k = i u_k \hat{c}_k + v_k \hat{c}_{-k}^\dagger \\ \hat{\Lambda}_k^\dagger = -i u_k \hat{c}_k^\dagger + v_k \hat{c}_{-k}, \end{cases} \quad (\text{A10})$$

where  $u_k$  and  $v_k$  are real coefficients, which fulfill the following relations

$$u_{-k} = -u_k, \quad v_{-k} = v_k, \quad u_k^2 + v_k^2 = 1. \quad (\text{A11})$$

The transformed Hamiltonian would only contain terms proportional to  $\hat{\Lambda}_k^\dagger \hat{\Lambda}_k$  when

$$A(k) + \frac{J \sin k}{4} \left( \frac{u_k}{v_k} + \frac{v_{-k}}{u_{-k}} \right) = 0. \quad (\text{A12})$$

In combination with (A11), we then have

$$u_k = \frac{\sin k}{\sqrt{2(1 - \cos k)}}, \quad v_k = \sqrt{(1 - \cos k)/2}. \quad (\text{A13})$$

Finally we end up with

$$\hat{\mathcal{H}} = E_k \left( \sum_k \hat{\Lambda}_k^\dagger \hat{\Lambda}_k - 1/2 \right), \quad (\text{A14})$$

with  $E_k = \cos 2\theta - \sin 2\theta \sin k$ .

## Appendix B: Determining the critical points by DMRG

To confirm our conclusion that the critical point locates at  $\theta_c = 0$  for  $U'/U < 1$ , we repeat the same calculations by Zhao et al.<sup>25</sup> but for Hamiltonian (2). The freedom at each site now is two, much smaller than that in the Hamiltonian (1), which allows us to obtain more accurate numerical data as well as larger sizes. In our DMRG calculations, we impose open boundary conditions.  $500 \sim 1200$  states are kept to ensure the truncation errors are smaller than  $10^{-7}$ . Moreover, we perform sweeps to improve the accuracy and to ensure the convergence of the ground-state energy per site to seven digits. The critical point  $\theta_c$  then is determined<sup>74,75</sup> through the entanglement entropy  $S_\rho$ , with  $S_\rho = \text{Tr} \rho \ln \rho$  via the reduced density matrix  $\rho$  of a half chain. In Fig. 9, we first plot the entanglement entropy versus  $\theta/\pi$  obtained with various chain lengths,  $L = 16, 32, 64, 128, 256, 512, 1024$  and 2048. Then, we determine  $\theta_m$ , where  $S_\rho$  is maximum, for each length, and deduce the critical point  $\theta_c$  in the thermodynamic limit by making an extrapolation with respect to  $1/L$ . In the inset, we show such an extrapolation for  $\theta_m$  with a variety of chain lengths, which can be fitted by a power-law function  $y = ax^b + c$ , with the best fitting parameters  $a = 0.783(4)$ ,  $b = 0.586(5)$  and  $c = 0.003(2)$ . Therefore, we conclude that within our error bar  $\theta_c = 0$ . One can see that  $\theta_c$  obtained by our two different methods are well consistent.

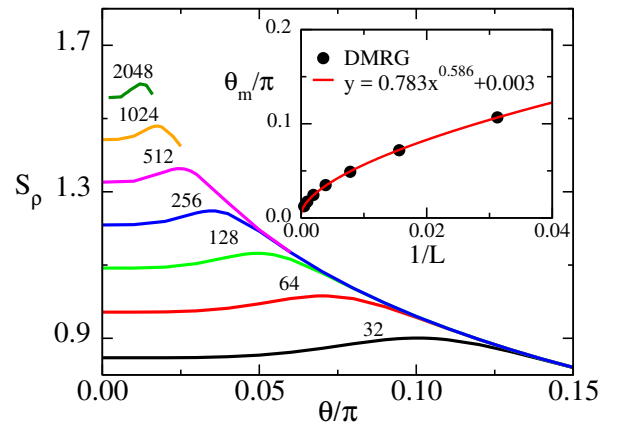


FIG. 9: (color online). Entanglement entropy  $S_\rho$  as a function of  $\theta$  for various system sizes are shown.  $\theta_m$ , where  $S_\rho$  shows up its maximum, are then extracted. Inset: finite-size scaling of  $\theta_m$  to determine the critical point.

<sup>\*</sup> These two authors contributed equally to this work.

<sup>†</sup> Electronic address: jizezhao@gmail.com

<sup>‡</sup> Electronic address: xiaoqunwang@ruc.edu.cn

<sup>1</sup> T. Giamarchi, *Quantum Physics in One Dimension* Oxford University Press, Oxford, England, 2004.

<sup>2</sup> F. D. M. Haldane, Phys. Rev. Lett. **45**, 1358 (1980); F. D. M. Haldane, J. Phys. C **14**, 2585 (1981).

<sup>3</sup> N. Motoyama, H. Eisaki, and S. Uchida, Phys. Rev. Lett. **76**, 3212 (1996).

<sup>4</sup> K. Hirakawa and Y. Kurogi, Prog. Theor. Phys. Suppl. **46**, 147 (1970).

<sup>5</sup> Y. Kono, T. Sakakibara, C. P. Aoyama, C. Hotta, M. M. Turnbull, C. P. Landee, and Y. Takano, Phys. Rev. Lett. **114**, 037202 (2015).

<sup>6</sup> R. J. Baxter, Phys. Rev. Lett. **26**, 832 (1971).

<sup>7</sup> E. Ercolessi, S. Evangelisti, F. Franchini, and F. Ravanini, Phys. Rev. B **83**, 012402 (2011).

<sup>8</sup> J. Cao, S. Cui, W. Yang, K. Shi, Y. Wang, Nuclear Physics B **886**, 185 (2014).

<sup>9</sup> D. Jaksch, H.-J. Briegel, J. I. Cirac, C. W. Gardiner, and P. Zoller, Phys. Rev. Lett. **82**, 1975 (1999).

<sup>10</sup> N. C. Collins, et al, Nature **425**, 973 (2003).

<sup>11</sup> L. M. Duan, E. Demler, and M. D. Lukin, Phys. Rev. Lett. **91**, 090402 (2003).

<sup>12</sup> F. Pinheiro, G. M. Bruun, J. Martikainen, and J. Larson, Phys. Rev. Lett. **111**, 205302 (2013).

<sup>13</sup> A. W. Glaetzle, M. Dalmonte, R. Nath, C. Gross, I. Bloch, and P. Zoller, Phys. Rev. Lett. **114**, 173002 (2015).

<sup>14</sup> R. M. W. van Bijnen and T. Pohl, Phys. Rev. Lett. **114**, 243002 (2015).

<sup>15</sup> Y. J. Lin, K. Jimenez-Garcia, and I. B. Spielman, Nature **471**, 83 (2011).

<sup>16</sup> P. J. Wang, Z. Q. Yu, Z. K. Fu, J. Miao, L. H. Huang, S. J. Chai, H. Zhai, and J. Zhang, Phys. Rev. Lett. **109**, 095301 (2012).

<sup>17</sup> L. W. Cheuk, A. T. Sommer, Z. Hadzibabic, T. Yefsah, W. S. Bakr, and M. W. Zwierlein, Phys. Rev. Lett. **109**, 095302 (2012).

<sup>18</sup> J.Y. Zhang, S. C. Ji, Z. Chen, L. Zhang, Z. D. Du, B. Yan, G. S. Pan, B. Zhao, Y. J. Deng, H. Zhai, S. Chen, and J. W. Pan, Phys. Rev. Lett. **109**, 115301 (2012).

<sup>19</sup> J. Radic, A. Di Ciolo, K. Sun, and V. Galitski, Phys. Rev. Lett. **109**, 085303 (2012).

<sup>20</sup> Z. Cai, X. F. Zhou, and C. J. Wu, Phys. Rev. A **85**, 061605 (2012).

<sup>21</sup> W. S. Cole, S. Z. Zhang, A. Paramekanti, and N. Trivedi, Phys. Rev. Lett. **109**, 085302 (2012).

<sup>22</sup> M. Gong, Y. Qian, M. Yan, V. W. Scarola, C. Zhang, Sci. Rep. **5**, 10050 (2015).

<sup>23</sup> X. Zhou, Y. Li, Z. Cai, and C. Wu, J. Phys. B **46**, 134001 (2013).

<sup>24</sup> Z. Fu, L. Huang, Z. Meng, P. Wang, L. Zhang, S. Zhang, H. Zhai, P. Zhang, J. Zhang, Nature Phys. **10**, 110 (2014).

<sup>25</sup> J. Zhao, S. Hu, J. Chang, P. Zhang, and X. Q. Wang, Phys. Rev. A **89**, 043611 (2014).

<sup>26</sup> J. Z. Zhao, S. J. Hu, J. Chang, F. Zheng, P. Zhang, and X. Q. Wang, Phys. Rev. B **90**, 085117 (2014).

<sup>27</sup> M. Piraud, Z. Cai, I. P. McCulloch, and U. Schollwöck, Phys. Rev. A **89**, 063618 (2014).

<sup>28</sup> Z. Xu, W. S. Cole, and S. Zhang, Phys. Rev. A **89**, 051604(R) (2014).

<sup>29</sup> S. Peotta, L. Mazza, E. Vicari, M. Polini, R. Fazio, and D. Rossini, J. Stat. Mech. (2014) P09005.

<sup>30</sup> C. Hamner, Y. Zhang, M. A. Khamehchi, M. J. Davis, and P. Engels, Phys. Rev. Lett. **114**, 070401 (2015).

<sup>31</sup> J. Zhao, S. Hu, and P. Zhang, Phys. Rev. Lett. **115**, 195302 (2015).

<sup>32</sup> E. Orignac, R. Citro, M. Di Dio, S. De Palo, M.-L. Chiofalo, New J. Phys. **18**, 055017 (2016).

<sup>33</sup> S. V. Syzranov, M. L. Wall, V. Gurarie, and A. M. Rey, Nat. Commun. **5**, 5391 (2014); M. L. Wall, K. Maeda, and L. D. Carr, New J. Phys. **17**, 025001 (2015).

<sup>34</sup> L.-N. Wu, X.-Y. Luo, Z.-F. Xu, M. Ueda, R. Wang, L. You, arXiv:1607.07005.

<sup>35</sup> I. Dzyaloshinsky, J. Phys. and Chem. Sol. **4**, 241(1958).

<sup>36</sup> T. Moriya, Phys. Rev. **120**, 91(1960).

<sup>37</sup> T. Kimura, Annu. Rev. Mater. Res. **37**, 387 (2007).

<sup>38</sup> S. Mhlbauer, B. Binz, F. Jonietz, C. Pfleiderer, A. Rosch, A. Neubauer, R. Georgii, and P. Böni, Science **323**, 915 (2009).

<sup>39</sup> X. Z. Yu et. al. Nature **465**, 901 (2010).

<sup>40</sup> S. Heinze et. al. Nature Phys. **7**, 713 (2011).

<sup>41</sup> N. Nagaosa and Y. Tokura, Nat. Nanotech. **8**, 899 (2013).

<sup>42</sup> A. Fert, V. Cros, and J. Sampaio, Nat. Nanotech. **8**, 152 (2013).

<sup>43</sup> V. L. Berezinskii, Sov. Phys. JETP **32**, 493 (1971); J. M. Kosterlitz and D. J. Thouless, J. Phys. C: Solid State Phys. **6**, 1181 (1973).

<sup>44</sup> D.C. Dender, P.R. Hammar, D.H. Reich, C. Broholm, and G. Aeppli, Phys. Rev. Lett. **79**, 1750 (1997).

<sup>45</sup> M. Kenzelmann, R. Coldea, D. A. Tennant, D. Visser, M. Hofmann, P. Smeibidl and Z. Tyliczynski, Phys. Rev. B **65**, 144432 (2002).

<sup>46</sup> M. Kenzelmann, Y. Chen, C. Broholm, D. H. Reich, and Y. Qiu, Phys. Rev. Lett. **93**, 017204 (2004).

<sup>47</sup> Y. Chen, M. B. Stone, M. Kenzelmann, C. D. Batista, D. H. Reich, and C. Broholm, Phys. Rev. B **75**, 214409 (2007).

<sup>48</sup> R. Feyerherm, S. Abens, D. Günther, T. Ishida, M. Meissner, M. Meschke, T. Nogami, and M. Steiner, J. Phys.: Condens. Matter **12**, 8495 (2000).

<sup>49</sup> S. A. Zvyagin, A. K. Kolezhuk, J. Krzystek, and R. Feyerherm, Phys. Rev. Lett. **93**, 027201 (2004).

<sup>50</sup> S. A. Zvyagin, A. K. Kolezhuk, J. Krzystek, and R. Feyerherm, Phys. Rev. Lett. **95**, 017207 (2005).

<sup>51</sup> M. Kohgi, K. Iwasa, J. Mignot, B. Fak, P. Gegenwart, M. Lang, A. Ochiai, H. Aoki, and T. Suzuki, Phys. Rev. Lett. **86**, 2439 (2001).

<sup>52</sup> X. Q. Wang and T. Xiang, Phys. Rev. B **56** 5061 (1997).

<sup>53</sup> R. J. Bursill, T. Xiang, and G. A. Gehring, J. Phys.: Condens. Matter **8**, L583 (1996).

<sup>54</sup> X. Q. Wang and L. Yu, Phys. Rev. Lett. **84**, 5399 (2000).

<sup>55</sup> T. Xiang, Phys. Rev. B **58**, 9142 (1998).

<sup>56</sup> A. Honecker, S. Hu, R. Peters, and J. Richter, J. Phys.: Condens. Matter **23**, 164211 (2011).

<sup>57</sup> J. Jedrzejewski, *Condensed Matter Physics in the Prime of the 21 Century, Phenomena, Materials, Ideas and Methods*. World Scientific, Singapore, 2008.

<sup>58</sup> J. Sirker, Int. J. Mod. Phys. B **26**, 1244009 (2012).

<sup>59</sup> K. A. Gschneidner, V. K. Pecharsky and A. O. Tsokol, Rep. Prog. Phys. **68**, 14791539 (2005).

<sup>60</sup> W. S. Bakr, P. M. Preiss, M. E. Tai, R. Ma, J. Simon, and

M. Greiner, *Nature* **480**, 500503 (2011).

<sup>61</sup> M. Vojta, *Rep. Prog. Phys.*, **66**, 2069 (2003).

<sup>62</sup> S. Sachdev and B. Keimer, *Physics Today*, **64**, 29 (2011).

<sup>63</sup> M. E. Fisher and A. N. Berker, *Phys. Rev. B* **26**, 2507 (1982).

<sup>64</sup> T. Kirkpatrick and D. Belitz, *Phys. Rev. B* **91**, 214407 (2015).

<sup>65</sup> T. Kirkpatrick and D. Belitz, *Phys. Rev. Lett.* **115**, 020402 (2015).

<sup>66</sup> S. Suzuki and A. Dutta, *Phys. Rev. B* **92**, 064419 (2015).

<sup>67</sup> D. Vollhardt, *Phys. Rev. Lett.* **78**, 1307 (1997); N. Chandra, M. Kollar, and D. Vollhardt, *Phys. Rev. B* **59**, 10541 (1999).

<sup>68</sup> D. S. Greywall, *Phys. Rev. B* **27**, 2747 (1983).

<sup>69</sup> G. E. Brodale, R. A. Fisher, N. E. Phillips, and J. Flouquet, *Phys. Rev. Lett.* **56**, 390 (1986).

<sup>70</sup> T. Adams, A. Chacon, M. Wagner, A. Bauer, G. Brandl, B. Pedersen, H. Berger, P. Lemmens, and C. Pfleiderer, *Phys. Rev. Lett.* **108**, 237204 (2012).

<sup>71</sup> Z. Wang, M. Schmidt, J. Fischer, V. Tsurkan, M. Greger, D. Vollhardt, A. Loidl and J. Deisenhofer, *Nat. Commun.* **5**, 3202 (2014).

<sup>72</sup> K. Okazaki, H. Wadati, A. Fujimori, M. Onoda, Y. Muraoka, and Z. Hiroi, *Phys. Rev. B* **69**, 165104 (2004).

<sup>73</sup> M. Greger, M. Kollar, and D. Vollhardt, *Phys. Rev. B* **87**, 195140 (2013).

<sup>74</sup> L. Amico, R. Fazio, A. Osterloh, and V. Vedral, *Rev. Mod. Phys.* **80**, 517 (2008).

<sup>75</sup> S. Ejima, H. Fehske, F. Gebhard, Kevin zu Münster, M. Knap, E. Arrigoni, and W. von der Linden, *Phys. Rev. A* **85**, 053644 (2012).